PAPER

Discrepancy between estimated and measured fusion product rates on MAST using TRANSP/NUBEAM

IOP Publishing | International Atomic Energy Agency Nuclear Fusion

Nucl. Fusion **59** (2019) 016006 (15pp) https://doi.org/10.1088/1741-4326/aaea19

Discrepancy between estimated and measured fusion product rates on MAST using TRANSP/NUBEAM

M. Cecconello[1], W. Boeglin[2], D. Keeling[3], S. Conroy[1], I. Klimek[1], R.V. Perez[2] and The MAST team[3]

[1] Department of Physics and Astronomy, Uppsala University, SE-751 05 Uppsala, Sweden
[2] Department of Physics, Florida International University, 11200 SW, Miami, FL 33199, United States of America
[3] United Kingdom Atomic Energy Authority, Culham Centre for Fusion Energy, Culham Science Centre, Abingdon, Oxon, OX14 3DB, United Kingdom of Great Britain and Northern Ireland

E-mail: marco.cecconello@physics.uu.se

Received 19 June 2018, revised 18 October 2018
Accepted for publication 22 October 2018
Published 19 November 2018

Abstract

Experimental evidence is presented of a discrepancy between the predicted and measured D–D fusion product rates on MAST. Both the neutron and proton production rates, measured independently with a neutron camera and charged fusion product detector array, are approximately 40% lower than those predicted by TRANSP/NUBEAM codes. This deficit is scenario independent and cannot be explained by uncertainties in the typical plasma parameters suspected for such discrepancies, such as electron temperature, the plasma effective charge and the injected neutral beam power. Instead, a possible explanation is an overestimate of the neutron emissivity due to the guiding centre approximation used in NUBEAM to model the fast ion orbits.

Keywords: spherical tokamak, MAST, fusion product deficit, TRANSP, NUBEAM

(Some figures may appear in colour only in the online journal)

1. Introduction

Recently, the discrepancy between the predicted and estimated neutron rates on JET has been the focus of a detailed study [1]. The authors of this study used an absolutely calibrated fission chamber (FC) [2] for measuring the neutron rate in several different JET plasmas and the TRANSP/NUBEAM codes [3, 4] to predict its expected values. The main conclusions of this study were that: (i) the measured neutron rate was smaller than the predicted one (the so-called neutron deficit) by a factor that ranged from 0%–50% depending on the plasma scenario; (ii) no clear correlation between the uncertainties in the main plasma parameter input to TRANSP/NUBEAM and the neutron deficit could be found; and (iii) that MHD activity was not the cause of this deficit. Possible causes for the observed neutron deficit suggested by the authors of that study included: unknown physical processes leading to large fast ion redistribution, calibration errors, uncertainties in the DD fusion reaction cross-sections and in the fast ion slowing down models used in NUBEAM.

In this work, we report similar observations on the mega ampere spherical tokamak (MAST) [5]. In addition to finding a neutron deficit between measurements and TRANSP/NUBEAM prediction, we have also measured a similar deficit in the proton production rates. The measured neutron and proton production rates on MAST are smaller than expected by a similar amount to the one found on JET—approximately 40%. Contrary to the observation in JET, however, the discrepancy in MAST is roughly the same for all investigated scenarios with and without the redistribution of fast ions due to MHD instabilities (when the anomalous transport of fast ions is accounted for). In a spherical tokamak, large fast ion populations, such as those originating from neutral beam injection heating, are not only responsible for the vast

Table 1. Summary of the plasma scenarios exhibiting a fusion product deficit. Neutron yield values indicate the maximum measured value by the fission chamber. Plasma configurations are a double null divertor (DND) and lower single null divertor (LSND). The charged fusion product detector (CFPD) was not available for all series.

Scenario	I_p (kA)	P_{NBI} (MW)	Y_{FC} ($\times 10^{13}$ s^{-1})	Conf.	CFPD	Notes
S1	800	1.50	3.0	DND	Yes	Quiescent MHD
S2	800	1.50	5.6	DND	Yes	Intermediate MHD
S3	800	2.75	9.4	DND	No	TAEs, large FBs and LLMs
S4	1000	3.40	15.0	DND	No	TAEs, FBs and LLMs
S5	630	1.50	5.0	LSND	No	TAEs, FBs and LLMs
S6	560	1.30	2.0	DND	Yes	Sawtooth

majority of all fusion reactions (the thermal reactivity is typically less than 5%), but they can excite MHD instabilities that cause their redistribution and loss. Fusion product diagnostics can therefore provide information on the confinement of fast ions, and the comparison between predictions and measurements on an absolute scale is thus of paramount importance in understanding the underlying physics used in the modelling codes, as well as in the testing of the code themselves in reference scenarios, such as those where no or little fast ion redistribution is expected.

This work presents new experimental evidence for the discrepancy between predicted and measured fusion products rates when using NUBEAM, which employs a guiding centre approximation together with a finite Larmor radius correction to model the full fast ion orbits. A systematic study of the possible causes for such a discrepancy, described in detail in this paper, has shown that the uncertainties in the experimental measurements and in the input data to TRANSP/NUBEAM cannot account for this discrepancy. Recent theoretical studies have shown that, for a spherical tokamak, the neutron emissivity along guiding centre approximate orbits is larger than the one calculated on full orbits [6, 7]. Contrary to conventional tokamaks, the confining magnetic field in a spherical tokamak is quite small, resulting in fast ions with energies in the tens of keV and large Larmor radii. This, in addition to the small size of MAST plasmas compared with the fast ion Larmor radii, combined with quite steep gradients in the plasma density and temperature, has been found to have an effect on the neutron emissivity. Modelling of the fusion products rates with full gyro-orbit codes is outside the scope of this work but, as a result of the conclusions reached here, is of extreme importance and will be carried out in a future work.

The paper is organized as follows. The database of MAST plasma scenarios and discharges and the fusion product diagnostics used in this study are presented in sections 2 and 3 respectively: in particular, section 3.2 describes the synthetic diagnostics used to estimate the expected fusion product rates starting from the neutron emissivity profiles calculated by TRANSP/NUBEAM. Section 4 is devoted to a comparison between the measurements and predictions, while the possible sources for the observed discrepancies are discussed in detail in section 5. Finally, the conclusions are presented in section 6.

2. Plasma scenarios

MAST is a medium sized spherical tokamak with an aspect ratio $R/a \approx 0.85/0.65 \approx 1.3$ and capable of sustaining plasma discharges with plasma current in the range 0.4–1.0 MA and temperatures as high as 2 keV in a very low toroidal magnetic field (typical values are in the range 0.45–0.6 T). Two neutral beam injectors (NBIs) provide additional heating (up to 3.5 MW) and are the main source of fast ions in MAST and the only source of neutron emission via the beam-thermal and beam–beam reactions up to a maximum neutron yield of about $Y \leqslant 2 \times 10^{14}$ s^{-1}. MAST is capable of a wide range of plasma scenarios with different divertor configurations, such as the up–down symmetric double null divertor (DND) and the down-shifted lower single null divertor (LSND) scenarios. It can be operated in L- and H-modes and the safety factor profile can be either monotonic or characterized by reversal in the core. MAST also exhibits a very rich set of MHD instabilities driven both by the background plasma equilibrium, such as sawtooth instability and edge localized modes, and by the presence of a large, super-Alfvénic fast ion population, such as toroidal Alfvén eigenmodes (TAEs), fish-bones (FBs) and long-lived modes (LLMs). The mechanism by which TAEs and FBs are excited is the free-energy made available by an NBI heating-driven large fast ion pressure with a very steep spatial gradient. These instabilities are responsible for the redistribution and loss of fast ions and the consequent reduction in the neutron emissivity [8]. From a fast ion perspective, MAST plasma discharges can then be divided in 'quiescent' scenarios characterized by no or very limited fast ion redistribution and in a 'non-quiescent' scenario where significant fast ion redistribution occurs. Table 1 summarizes the database of discharges used in this study which cover a wide range of plasma currents, from 0.5–1.0 MA with different levels of NBI heating, from 1.3–3.4 MW, in DND and LSND configurations grouped in six scenarios. Scenarios S_1 and S_6 are quiescent scenarios where little or no fast ion redistribution occurs during parts of the discharge. In the case of scenario S_6, strong fast ion redistribution occurs at the sawtooth crash but the fast ion population recovers fairly quickly so that in the inter-sawtooth crash period, no redistribution occurs. Scenarios S_2–S_4 are characterized by different levels of fast ion redistribution. Scenario S_5, which exhibits instabilities very similar to those of S_3 and S_4, is included in the database to

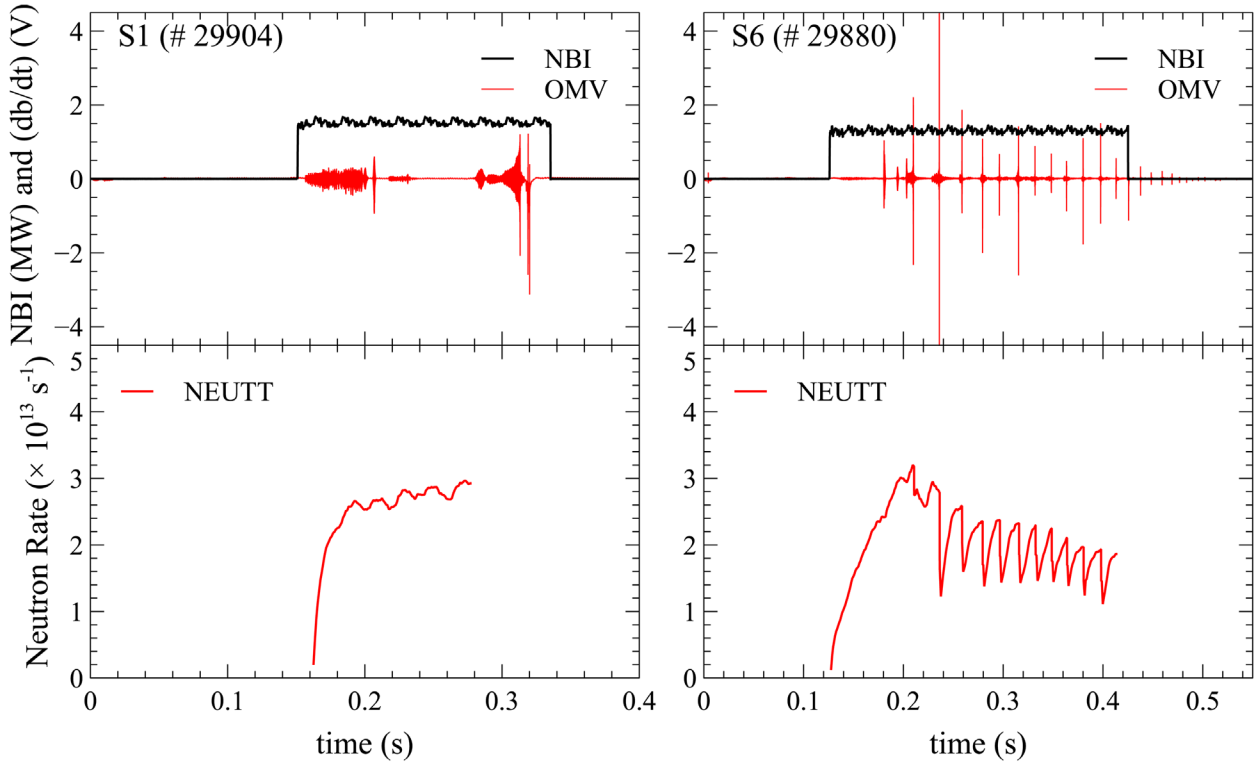

Figure 1. Time traces of the NBI heating signal (black) and of a Mirnov pick-up coil (red) for a representative plasma discharge for two scenarios: quiescent plasma (left panels), with reference to a perturbation-free time interval between 0.20 and 0.28 s; saw-teething plasma (right panels). The neutron rate predicted by TRANSP/NUBEAM is shown in the bottom panels.

provide a historical perspective on the fusion product discrepancy as the discharges in S_5 were carried out almost two years before those of all the other scenarios. An example of the different nature and level of MHD activity in quiescent and non-quiescent scenarios is shown in figure 1 where the signal from a Mirnov pick-up coil is shown for selected discharges for scenarios S_1 and S_6, together with the time trace of the NBI power and the corresponding TRANSP/NUBEAM simulated neutron rate. Thanks to MAST high reproducibility, all the discharges within each scenario are almost identical: this has been exploited to measure the neutron emissivity profile, as discussed in section 3. Table 2 lists the discharges included in each scenario, with those in bold being modelled with the codes TRANSP/NUBEAM (see section 3.2) as representative discharges for each scenario.

Table 2. List of plasma discharges used in this study. The representative plasma discharge for each scenario that has been modelled in TRANSP is in bold.

Scenario	Pulse numbers
S1	**29 904**, 29 905, 29 906, 29 908, 29 909, 29 910
S2	29 222, 29 917, **29 924**, 29 928, 29 929, 29 931
S3	29 975, **29 976**, 29 980
S4	29 132, 29 181, 29 207, 29 208, 29 209, **29 210**, 29 359
S5	27 932, 27 934, 27 935, 27 936, **27 938**
S6	29 879, **29 880**, 29 881, 29 882, 29 884, 29 885

3. Fusion product diagnostics and TRANSP/NUBEAM simulations

The two principal diagnostics for this study are a neutron camera (NC) and the charged fusion product detector array (CFPD). A detailed description of these two diagnostics can be found in [9, 10]. An overview of the plasma regions probed by the NC and the CFPD is shown in figure 2. The NC views the plasma along two collimated lines of sight on the equatorial plane through a thin stainless steel flange; two additional lines of sight look at the plasma 20 cm below the mid-plane. The NC sight-lines impact parameter p can be changed in between plasma discharges, thus allowing the measurement of the neutron emissivity covering the entire plasma region from the inboard to the outboard side. The NC detectors consist of liquid scintillators (EJ-301 type) coupled to photo-multipliers. Each detector is equipped with a ^{22}Na source and connected to an LED source and both are used to correct for gain shifts in the PMT gain due to high count rates (CRs) and the stray magnetic field. The light output of the EJ-301 scintillator to incident γ-rays and neutrons has been provided by the detector manufacturer. The efficiency of the detectors to 2.45 MeV neutrons from the DD fusion reaction has been determined by a combination of MCNP simulations [11] and absolute calibration of the acquisition energy threshold in an MeV electron equivalent using multiple standard γ-ray sources. The results of such simulations agree with similar Monte Carlo simulations available in the literature validated by measurements of the efficiency to mono-energetic neutron beams [12–16]. The efficiency so determined for the NC detectors is $\epsilon = 13\%$. The attenuation of the neutron flux through the thin stainless

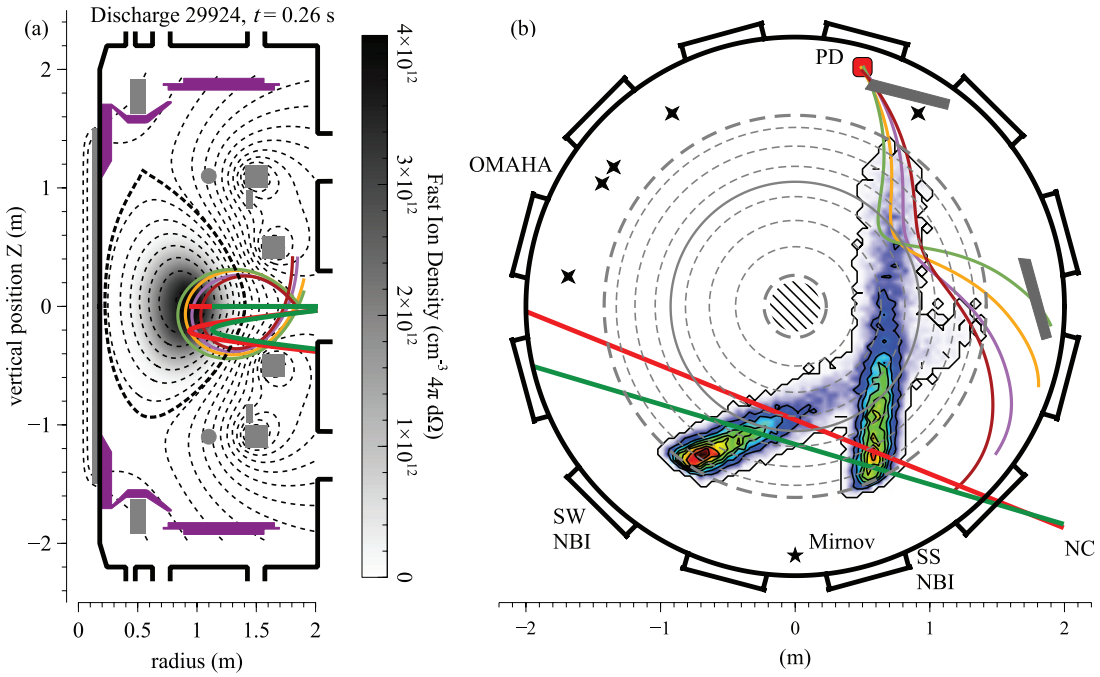

Figure 2. Overview of the sight-lines looking at the plasma core for the neutron camera (red and green solid lines) and for the charged fusion product detector (pale green, yellow, magenta and brown) on a poloidal cross-section (*a*) and on the equatorial plane (*b*), together with the slowed down fast ion density shown in (*a*) and the fast ion birth location from the neutral beam injection in (*b*). The location of the CFPD on the equatorial plane is indicated by the red square.

steel flange has also been estimated via MCNP simulations resulting in a transmission coefficient $\eta = 0.904$.

The CFPD consists of four silicon surface-barrier (SSB) diodes mounted inside a shielding case with collimated views of the plasma and shielded against light and x-ray radiation by a 0.8 μm thick aluminium foil. The active layer at 100 μm thick is designed to fully stop the 3 MeV protons while being insensitive to neutrons. The CFPD is mounted on a linear manipulator arm which provides limited radial scan capabilities, from $R = 0.75$ m to $R = 1.05$ m, along the mid-plane. An example of the typical trajectories of the 3 MeV protons from the DD reaction reaching the detectors, calculated for the specific magnetic equilibrium reconstructed with EFIT [17], are shown in figure 2. Two out of the four channels in the CFPD are partly shadowed by one of the NBI dumps, as shown in figure 2: in this study, therefore, only results from the two channels not affected by the shadowing are presented. This non-optimal experimental set-up was due to the limited time available for the installation of the CFPD on MAST (only one port on the machine could be made available) and for carrying out these measurements before MAST went into shutdown. The efficiency of the CFPD for 3 MeV protons is approximately $\epsilon_{SSB} = 97\%$. The efficiency of SSB with the proper minimum depletion depth is in general accepted to be 100% for a properly working detector. Charged particle detection losses are mostly due to missed proton pulses due to either large electrical noise signals or pile-up events (for example, pulses that are less than approximately 400 ns apart and are therefore not identified as two individual pulses). In order to determine such an effect on the detection efficiency, artificial signals have been added to real data and analysed: the number of simulated event losses at the measured particle rate has then been used as a measure of the detection efficiency.

In addition to the NC and CFPD, MAST is equipped with an absolutely calibrated ^{235}U FC used to monitor the global neutron yield Y_n with a time resolution of 10 μs [18]. The calibration of the FC was carried out once at the very beginning of the MAST operations and its calibration has been tracked through the years with a neutron activation system.

3.1. Synthetic diagnostics

The NC and CFPD measure the CR with which neutrons and protons are detected. In order to compare the measured CRs with the theoretical predictions, synthetic diagnostics have been developed. The synthetic diagnostics combine the plasma equilibrium, the neutron emissivity $\varepsilon_n(R,Z)$ on a poloidal cross-section calculated by TRANSP/NUBEAM with the geometry of the lines of sight and the detectors' response function (including their efficiency) to provide the expected neutron and proton CRs. A detailed description of the NC synthetic diagnostic can be found in [19]. The predicted NC CR for a given impact parameter p, $\nu_n(p)$, is given by:

$$\nu_n(p) = \eta\epsilon \sum_{i,j} \varepsilon_n(R_{i,j}, Z_{i,j})\Omega(p; R_{i,j}, Z_{i,j}) \quad (1)$$

where $\Omega(p; R_{i,j}, Z_{i,j})$ is the 2D mapping on the poloidal cross-section of the 3D solid angle subtended by a volume element of the plasma multiplied by its volume for an NC detector viewing the plasma with tangency radius p. The summation is over all volume elements used in NUBEAM to estimate the

neutron emissivity on a poloidal cross-section. The quantity $\Omega(p; R_{i,j}, Z_{i,j})$ is calculated with a Monte Carlo code which implements the full 3D geometry of MAST and of the NC. The code has been validated against analytical calculations and a good agreement has been found (relative difference less than 5%). It has already been observed in a previous work [19] that the profile shape of the NC CR as a function of the impact parameter $\nu_{\rm NC}(p)$ was in good agreement with $\nu_{\rm n}(p)$ but agreement on the absolute magnitude could only be achieved if the latter was multiplied by a constant scaling factor $k \approx 0.7$, that is $\nu_{\rm NC}(p) = k\nu_{\rm n}(p)$. A systematic validation of the neutron emissivity profile $\varepsilon(R, Z)$ calculated by NUBEAM was then carried using the directional relativistic spectrum simulator (DRESS) code [20]. A good agreement was found between DRESS and NUBEAM neutron emissivities (relative difference less than 1%). DRESS can model the energy spectra of the products from fusion reactions involving two reactants with arbitrary velocity distributions employing fully relativistic kinematic equations to calculate the energy of the fusion products. The inputs for DRESS are the equilibrium magnetic field and the reacting fuel ion velocity distribution function, which in this validation was provided by NUBEAM itself.

The simulation of the CFPD CRs is based on the same TRANSP/NUBEAM simulations used for the NC. In this case, the proton emissivity $\varepsilon_{\rm p}(R, Z)$ is assumed to be equal to the neutron one, both in its spatial distribution and intensity and that protons do not undergo collisions between their birth and the detector. The probability for such a reaction along a path length of 400 m in a plasma density of 6×10^{19} m^{-3} has been estimated to be of the order of approximately 10^{-7}. The spatial distribution is identical since the fuel and fast ion spatial distribution is the same for both reaction channels. The intensity of the neutron and proton emissivities can be assumed to be identical since the ratio of the thermal emissivity varies between 1.02 and 1.03 in the ion temperature range of interest ($T_{\rm i} < 1.0$ keV) and the ratio of the beam-thermal cross-sections for the beam-target reactions D(d,n)^{3}He and D(d,p)T varies between 0.97 and 0.98 for the fuel ion and NBI energies of the plasma scenarios here studied [21]. Interpolation over the *RZ* plane is carried out to estimate the proton emissivity $\varepsilon_{\rm p}(R, Z)$ along the proton trajectories which are backward calculated with a full orbit following code in the equilibrium magnetic field calculated via EFIT. The full-orbits are backtracked starting from the CFPD position until they intersect the vessel walls, the coils and other obstacles: the path length of all simulated orbits has never exceeded 400 m in this analysis. For each detector–collimator pair, a large number of orbits are calculated (between 81 and 6) to take into account the non infinitesimal size of the field of view by dividing the collimator and detector areas in 3×3 or 5×5 arrays. The expected CFPD CRs $\nu_{\rm p}$ are then given by the integration of the proton emissivity along each orbit as:

$$\nu_{\rm p} = \epsilon_{\rm SSB} \sum_i A_{\rm i} \int_{\ell_{\rm i}} \varepsilon_{\rm p} \left[R(\ell), Z(\ell)\right] \, {\rm d}\ell \qquad (2)$$

where ℓ is the position of the proton along its orbit, $A_{\rm i}$ is the phase space acceptance [22] for this bundle and the summation is carried out over all the orbit bundles.

3.2. TRANSP/NUBEAM simulations

The quality of TRANSP/NUBEAM simulation depends on two key factors: the quality of the input plasma parameters and the appropriate choice and combination of the different parameters that control how the simulation is carried out. The input plasma parameters in TRANSP/NUBEAM were calculated via the MC^3 pre-processor which takes the input global plasma parameters from different MAST plasma diagnostics, such as Thomson scattering for the electron density and temperature profiles, bremsstrahlung radiation emission diagnostic for the plasma effective charge, CXRS spectroscopic diagnostics for impurity rotation, the neutron rate from the FC, H_α edge measurements for the neutral density at the plasma boundary and D_α camera images for the plasma edge position, the plasma current and the NBI power, as well as all the data from the magnetic flux loops and pick coils necessary for the reconstruction of the plasma equilibrium and motional Stark effect measurements for constraining the internal magnetic field structure. The magnetic equilibrium is reconstructed in MC^3 by EFIT by leaving the core pressure profile unconstrained to account for the fact that in MAST, the fast ion pressure is a significant contribution not measured by the Thomson scattering system which is only sensitive to thermal electron pressure. The experimental plasma global parameters, each with its own temporal and spatial resolution, are mapped by MC^3 onto the EFIT equilibria on a single common time axis and interpolated on a single normalized radial coordinate. Profile regularization is used to reproduce, as realistically as possible, the plasma profiles by removing, for example, unphysical features such as spikes. The preprocessor also takes care of preparing the NBI input files required by TRANSP/NUBEAM as well as setting up all the TRANSP/NUBEAM modelling options. The files produced by MC^3 are then edited to tweak the simulation, for example, by including the options controlling the anomalous fast ion diffusion coefficient or to simulate variation in the plasma input profiles. One important option used in the TRANSP simulation is the use of its internal equilibrium solver (TEQ) constrained solely by the vacuum toroidal field, the plasma boundary from EFIT, the plasma current and an initial estimate of the q-profile form EFIT. The equilibrium thus calculated is then self-consistent in that internal power balance is used to calculate the total pressure (thermal plus kinetic). One limitation of this approach, and consequently of the simulations carried out here, is that, at present, TRANSP cannot properly model poloidal asymmetries in the equilibria caused by toroidal flow, as discussed in [23] and [24]. Resolving or addressing such limitations is outside the scope of this paper. As for NUBEAM, several options are of importance for the calculation of the fast ion distribution and of the neutron emissivity: (i) the number of test particles used in the Monte Carlo simulation; (ii) the

anomalous fast in diffusion coefficient; (iii) the correction to the guiding-centre orbit calculations due to the finite Larmor radius; (iv) the FBs and sawtooth models; (v) toroidal field ripples, and (vi) the selection of several plasma state output files which contain the time averaged four-dimensional fast ion distribution (in R, Z, energy and pitch angle), the non-flux averaged neutron emissivity (in R, Z) and the magnetic field which is required for DRESS. A large number of Monte Carlo test particles is required to obtain high quality fast ion distributions (with low statistical variance). The anomalous fast ion diffusion coefficient allows us to simulate the redistribution of fast ions. Toroidal field ripples can cause fast ion orbit losses. These are discussed in detail in the following sections. All the simulations used in this study have been carried out with the finite Larmor radius correction applied to the guiding-centre orbits calculated by NUBEAM: this is necessary due to the non-negligible Larmor radius of fast ions in MAST. Without this correction in place, the predicted neutron rate is higher than in the case when the correction is applied. The FBs and sawtooth models have been implemented only for scenarios S_3 and S_6 respectively. The methodology used to simulate these scenarios, using the measurements from fast ion diagnostics as constraints, are detailed in [8, 19, 25] and [26]. All the fast ion distributions and neutron emissivities used in this study have been averaged over a period of 3 ms, which is a reasonable compromise between good statistics and constant plasma conditions.

A standard output of TRANSP/NUBEAM is the total neutron yield Y_n which is usually compared with the one measured by an absolutely calibrated FC, Y_{FC}. On MAST, for quiescent scenarios, good agreement is found between the two if Y_{FC} is multiplied by 0.9—a correction factor which accounts for drifts in the FC since its absolute calibration. In the case of non-quiescent scenarios, $Y_n > Y_{FC}$, an observation which is usually interpreted as a reduction in the fast ion confinement due to energetic particle modes. Agreement between the two is recovered in TRANSP/NUBEAM by introducing an anomalous fast ion diffusion coefficient D_a to account for the redistribution of fast ions. The anomalous fast ion diffusion coefficient can be specified by the user in the input file to have an energy, space and time dependency which is typically adjusted so that the predicted and measured neutron yields match. On MAST, good agreement can be obtained between the predicted and measured neutron yields using a D_a which is constant in space and energy and varies only in time: typical values for D_a range from 0 $m^2\ s^{-1}$ for quiescent scenarios up to 3 $m^2\ s^{-1}$ for non-quiescent scenarios.

The neutron emissivity used in equation (1) is calculated by NUBEAM as a non flux-surface averaged quantity in contrast to the standard output which is flux-surface averaged. In order for the neutron emissivity to be calculated with low statistical variance, each TRANSP/NUBEAM simulation discussed in this work has been carried out with a large number of Monte Carlo model particles (5×10^4) representing the NBI fast ions, resulting in long computational times. The implication of this will be discussed in further detail in section 4.2. As for the total neutron yield, good agreement between Y_n and Y_{FC} is achieved, even when a low number of Monte Carlo model particles (10^3) is used in the TRANSP/NUBEAM modelling. For example, the standard deviation in the relative difference of Y_n between simulations with 10^3 and 5×10^4 particles is approximately 0.025, but the required simulation time for the former is approximately 30 times shorter.

4. Simulations versus observations: a systematic study

In this section, the evidence of a systematic discrepancy between the predicted and measured CRs for the fusion products is presented. Predicted 2.45 MeV neutron and 3 MeV proton CRs have been estimated from TRANSP/NUBEAM simulations with a large number of Monte Carlo particles at selected times during the plasma discharge for all representative pulses listed in table 2. The neutron emissivity at these selected times is the average over a 3 ms time interval for the NC and between 5 and 20 ms for the CFPD. The quiescent scenarios, discussed in section 4.1, are characterized by little or no fast ion redistribution and therefore have been simulated setting $D_a = 0\ m^2\ s^{-1}$. The fusion product discrepancy was also found in a wider range of plasma scenarios characterized by non-quiescent MHD activity. These scenarios were simulated first with no anomalous fast ion diffusion and then by adjusting D_a to match the neutron yield measured by the FC, as discussed in detail in section 4.2.

4.1. Quiescent MHD scenarios

Figure 3 shows two typical examples of the discrepancy observed between predicted neutron CRs ν_n and those measured by the neutron camera, ν_{NC}. The profile $\nu_{NC}(p)$ is obtained by combining all the plasma discharges for each scenario while the predicted profile $\nu_n(p)$ is based on the TRANSP/NUBEAM modelling of plasma discharges #29 904 and #29 880. The results presented in figure 3 highlight the fact that TRANSP/NUBEAM simulations are able to correctly reproduce the shape of the neutron camera CR profile but not its amplitude. Good agreement between the predicted and measured CRs is achieved if ν_n is multiplied by a factor $\bar{k} = 0.67 \pm 0.02$ for S_1 and $\bar{k} = 0.65 \pm 0.02$ for S_2. The quantity $\bar{k}$ is the average of the ratios $k(p_i) = \nu_{NC}(p_i)/\nu_n(p_i)$, while the quoted uncertainty, in this and all the following sections, is the standard deviation of the mean. This discrepancy cannot be explained, even when taking into account the uncertainties in the input parameters to TRANSP/NUBEAM. The plasma parameters that affect the neutron emissivity are the electron temperature T_e and the effective charge Z_{eff} while the electron density n_e and the ion temperature T_i have a negligible effect [19]. When a relative uncertainty of 10% is included in both T_e and Z_{eff} (typical values on MAST) the discrepancy between ν_{NC} and ν_n is still larger than the error bars for both scenarios, as shown in figure 3 by the dashed lines. In order to match ν_n to ν_{NC}, it would be necessary to either double the value of the core Z_{eff} (from 1.5 to 3.1) or reduce the electron temperature by approximately 26%. In both cases, these are variations much larger than those that are deemed

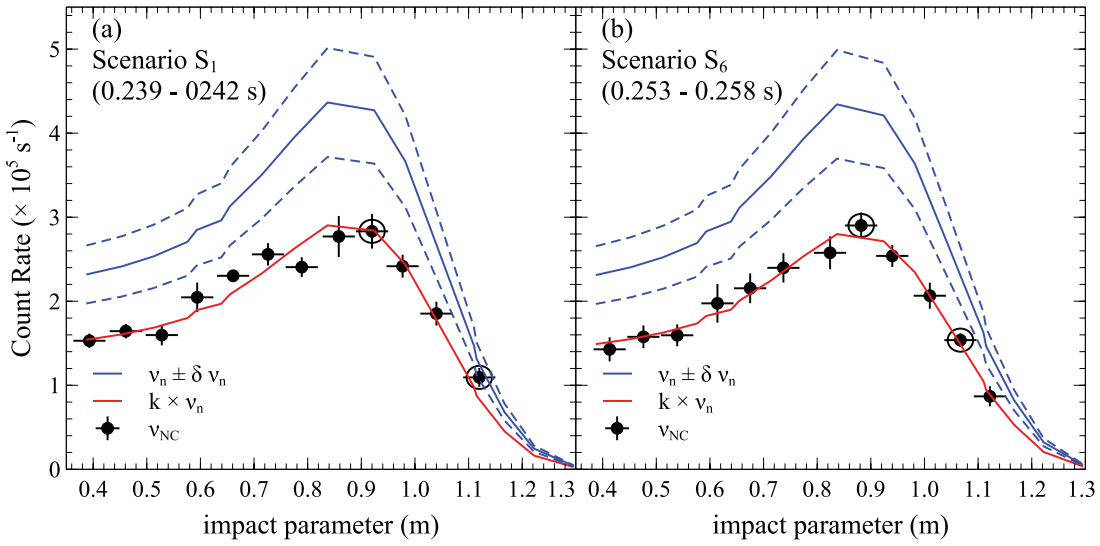

Figure 3. Comparison between measured (solid circles) and predicted (continuous lines) neutron camera CRs for scenario S_1 and S_6 in (*a*) and (*b*) respectively in selected time intervals. Predicted CRs ν_n (solid blue line) are shown with their uncertainties (dashed blue lines) and multiplied by the scaling factor k (red lines): in this case, $\bar{k} = 0.665$ (*a*) and $\bar{k} = 0.645$ (*b*). The open circles indicate the experimental data belonging to the reference pulses, #29 904 and #29 880 respectively.

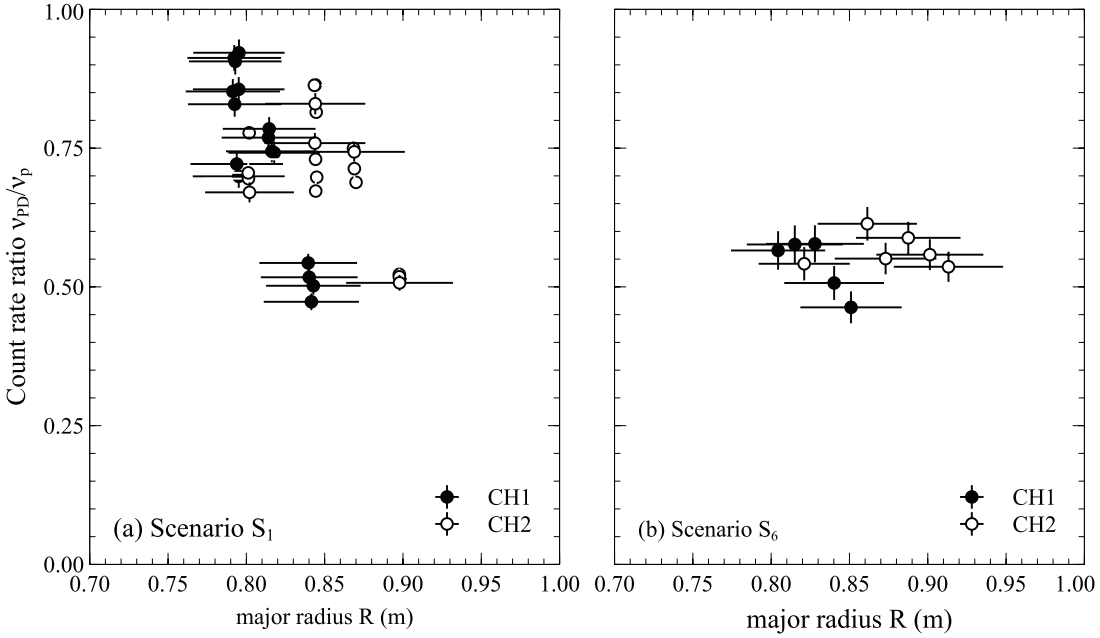

Figure 4. Ratios between the charged fusion product detector CRs of the proton emission ν_{PD} measured by two channels to those predicted by TRANSP ν_n for four plasma discharges of scenario S_1 for $t \approx 0.21, 0.22, 0.24$ and 0.26 s in (*a*) and for five plasma discharges of scenario S_6 in (*b*) for $t \approx 0.25$ s, before a sawtooth crash. The horizontal bars indicate the range of mid-plane radii covered by each CFPD detector channel.

acceptable given their uncertainties: the relative uncertainty of the electron temperature has been determined to be less than 5% [27] and less than 30% for Z_{eff} [28]. Additional TRANSP/NUBEAM simulations have been performed where the NBI energy and densities were changed. In such a case, in order to reproduce the experimental results, the NBI energy should be reduced from 60 to 52.5 keV or the beam density by 35%. These large variations are also beyond their accepted uncertainties and are therefore not credible [29]. As a final comment on the neutron CRs, it is worth nothing that the predicted CRs are based only on the contribution of uncollided neutrons, that is neutrons that are emitted from the plasma and reach the detector without making any collision. A fraction of the measured CRs, however, is due to collided neutrons since the detectors cannot discriminate between uncollided and collided neutrons. The fraction of scattered neutrons has been estimated to be less than 10% for impact parameters $p \leqslant 1.1$ m [9]. As a result, the actual ratio $\bar{k}$ would be reduced by a similar amount giving $k \approx 0.59$, indicating an even larger discrepancy between the experiment and model. A similar discrepancy is observed for the CFPD CRs of the 3 MeV protons ν_{PD}, as shown in figure 4. The profile of the ratio ν_{PD}/ν_p is

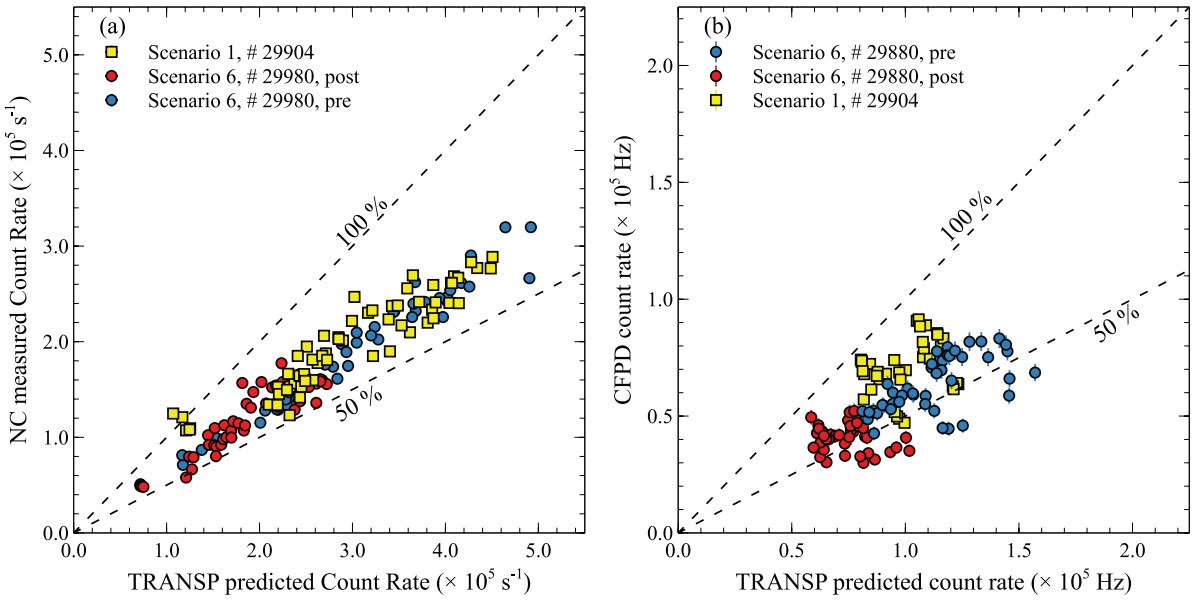

Figure 5. Comparison between TRANSP predicted and measured CRs by the neutron camera (*a*) and the charged fusion product detectors (*b*) for scenarios S_1 and S_6. TRANSP predictions with no anomalous fast ion diffusion coefficient. Each experimental data point represents the ratio between individual NC/CFPD channels and the TRANSP predicted CRs for selected times during the plasma discharge. The labels 'pre' and 'post' refer to the time intervals before and after a sawtooth crash.

shown for selected time intervals for both S_1 and S_6: in this case, we observe $\bar{k} = 0.72 \pm 0.02$ and $\bar{k} = 0.57 \pm 0.01$. It is worth mentioning that in the case of S_6, the deficits in ν_{NC} and ν_{PD} are not affected by the sawtooth crashes, i.e. the deficit is approximately the same as that indicated when measured before, and a few ms after, each sawtooth crash (the neutron rate is averaged in 3 ms time intervals, while the proton rate is averaged in 5 ms time intervals).

Finally, figure 5 shows the scaling between TRANSP/NUBEAM predictions and measured CRs for each pulse, time and impact parameter (for the NC) and radial position (for the CFPD). As can be seen, most of the experimental measurements are characterized by a deficit between 0% and 50% with an average value of $k = 0.64 \pm 0.02$ and 0.62 ± 0.09 for the NC and the CFPD respectively. A few NC data points for scenario S_1 fall on the 100% line: these data points all come from measurements at large impact parameter $p \gtrsim 1.1$ m. The reason for this deviation from the overall trend is not clear but it might be due to the peculiarity of this scenario since such deviations are not observed in all other scenarios for similar impact parameters.

4.2. Non-quiescent scenarios

A comparison between the predicted and measured CRs ν_n and ν_{NC} is carried out firstly by setting $D_a = 0\ m^2\ s^{-1}$, even if fast ion redistribution and the associated reduction in the neutron emissivity is expected. The rationale for this is to see by how much the TAEs, FBs and LLMs affect the scaling factor k, thus providing an estimate of the redistribution of fast ions based only on the neutron camera measurements. An example of this comparison is shown in figures 6(*a*) and (*b*) for scenarios S_3 and S_4 respectively. For the time intervals indicated, the scaling factor is $\bar{k}_a = 0.47$ and $\bar{k}_a = 0.39$ respectively, where the index 'a' indicates that this scaling factor applies in the presence of anomalous fast ion redistribution; as expected, we observe that $k > k_a$. Note that in these scenarios too, the simulated CR profile well matches the shape of the experimentally measured one. The dependency of $\bar{k}_a$ on the MHD activity is shown in figures 6(*c*) and (*d*) where the evolution in time of the RMS of the signal of a Mirnov pick-up coil is plotted together with $\bar{k}_a(t)$ for the corresponding scenarios. In the case of S_3, initially $\bar{k}_a \approx 0.4$ when strong MHD activity is present, first in the form of TAEs (from 0.1–0.17 s), followed by FBs (from 0.17–0.24 s) which are followed by the LLM up to 0.3 s. For $t > 0.3$ s, the perturbation is reduced in amplitude and, correspondingly, the scaling factor $\bar{k}_a$ tends towards the values of k observed for quiescent scenarios, i.e. $\bar{k}_a \approx 0.65$. In the S_4 case instead, as the MHD activity persists throughout the entire pulse, k_a remains suppressed at a level of approximately 0.4. When the scaling factor k_a is evaluated for individual impact parameters, times and plasma discharges, the effect of the fast ion redistribution results in a discrepancy between 50% and 70% with a different scaling than the one for the quiescent scenarios.

The neutron emission for the representative plasma discharges for scenarios S_2–S_5 was then recalculated introducing a non-zero, time dependent, anomalous diffusion coefficient in the TRANSP/NUBEAM simulations. For S_3 and S_5, the FB loss model present in NUBEAM was also used in order to correctly reproduce the sharp drops in the neutron yield at the onset and during the chirping down phase of these instabilities. The level and time dependence of the anomalous diffusion was obtained by adjusting D_a so that $Y_n(t) \simeq 0.9 \times Y_{FC}(t)$ rather than trying to match $\nu_n(p,t)$ with $\nu_{NC}(p,t)$. This was done for two reasons. The first is due to the fact that a manual iterative approach was used to adjust D_a: an agreement between the measured and predicted neutron yield could be achieved

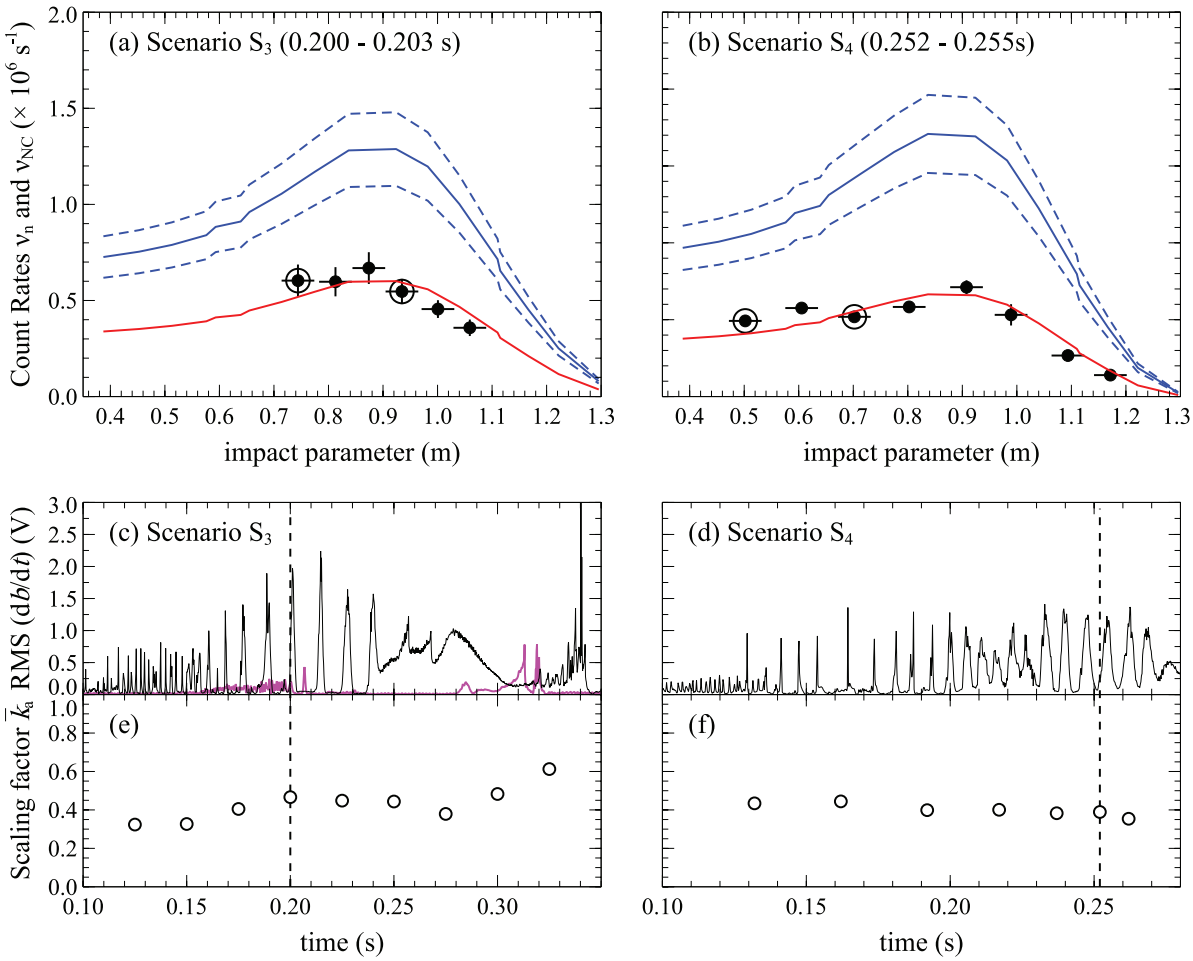

Figure 6. Comparison between measured (solid circles) and predicted (continuous lines) neutron camera CRs for scenario S_3 and S_4 in (*a*) and (*b*) respectively. The open circles indicate the experimental data belonging to the reference pulses, #29 976 and #29 210 respectively. Predicted CRs ν_n (solid blue line) are shown with their uncertainties (dashed blue lines) and multiplied by the averaged anomalous scaling factor $\bar{k}_a$ (red lines): $\bar{k}_a = 0.466$ (*a*) and $\bar{k}_a = 0.389$ (*b*). The time evolution of the RMS of the Mirnov coil signals is shown in (*c*) (black line for #29 976 and in magenta for pulse #29 904 of scenario S_1) and (*d*) for scenario S_4 (#29 210) respectively. (*e*) and (*f*) The corresponding evolution of the averaged anomalous scaling factor $\bar{k}_a$. The vertical dashed lines indicate the times of the CR profiles shown in (*a*) and (*b*).

fairly quickly as the number of Monte Carlo particles required is quite small. The second and most important motivation is that matching $\nu_n(p,t)$ with $\nu_{NC}(p,t)$ would have required D_a values uncommonly higher than those observed in NSTX (1–2 $m^2\ s^{-1}$) [30, 31] and ASDEX-U (about 1 $m^2\ s^{-1}$) [32] in the presence of similar MHD activity. Good agreement between Y_n and Y_{FC} is obtained with D_a varying between 0 and 2.8 $m^2\ s^{-1}$. With the condition $Y_n(t) \simeq 0.9 \times Y_{FC}(t)$ achieved, new simulations were carried out with large numbers of Monte Carlo particles and the non-flux averaged neutron emissivity was calculated at selected times. Figures 7(*a*)–(*d*) show the comparison between the recalculated ν_n and ν_{NC} for selected times for scenarios S_2–S_5. As can be seen, in all four cases the CR profiles agree both in shape and amplitude with a scaling factor $\bar{k}$ ranging from 0.58–0.68 that is very similar to the one in the quiescent scenarios. The case of scenario S_5 is of particular interest because it confirms that this discrepancy has been present at the same level well before the plasma discharges for the other scenarios were carried out. The same high statistic simulation used for the neutron measurement analysis for scenario S_2 was then used to calculate the ratio ν_{PD}/ν_p which is shown in figure 7(*e*), resulting in an average scaling factor of $k = 0.71 \pm 0.01$, thus confirming the presence of a deficit in both channels of the DD fusion reaction. In conclusion, the deficit between the predicted and observed CRs is consistently between 0% and 50% for both fusion products alike (neutrons and protons) for all different scenarios with and without fast ion redistribution. These observations are summarized in table 3 and in figure 8 for both quiescent and non-quiescent scenarios (when the anomalous fast ion diffusion is included in the TRANSP/NUBEAM modelling).

4.3. Regression analysis

The analysis in the previous sections is based on the ratio of two random normal variables which might not be normally distributed. For this reason, the scaling factor k has also been calculated by a weighted least square (WLS) regression using, as a model function, $y = kx$ where y is the measured CR for the NC and CFPD and x is the TRANSP predicted one. The weights in y come from the experimental uncertainty in the CRs, while the independent variable x is assumed to have no

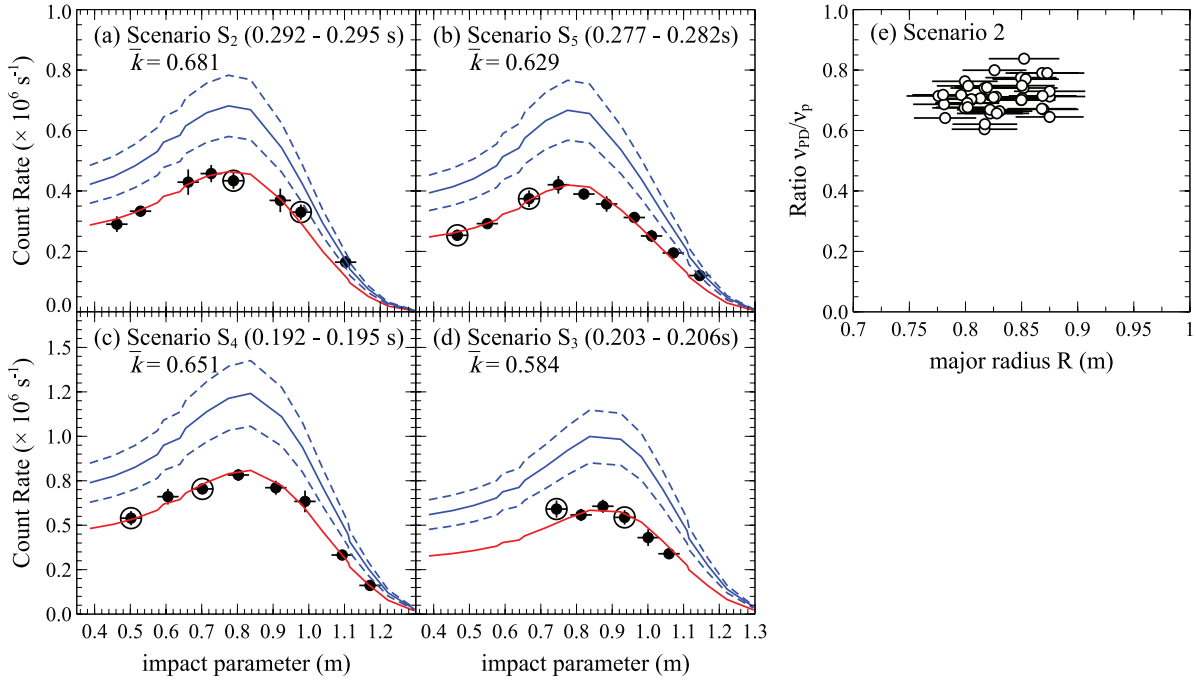

Figure 7. (*a*)–(*d*) Comparison between measured (solid circles) and predicted (continuous lines) neutron camera CRs for scenarios S_2–S_5; predicted CRs ν_n (solid blue line) are shown with their uncertainties (dashed blue lines) and multiplied by the averaged scaling factor $\bar{k}$ (red lines). The open circles indicate the experimental data belonging to the reference pulses, #29 924, #27 938, #29 976 and #29 210 respectively. (*e*) Ratios between the CFPD CRs ν_{PD} measured by two channels to those predicted by TRANSP ν_p for the plasma discharges of scenario S_2.

Table 3. Best estimate of the scaling factor for each scenario from neutron camera data (k_{NC}) and the CFPD (k_{PD}). The labels 'pre' and 'post' refer to the time intervals before and after a sawtooth crash. The horizontal dash '—' indicates that CFPD measurements are not available.

Scenario	k_{NC}	k_{PD}
S1	0.69 ± 0.01	0.72 ± 0.02
S2	0.70 ± 0.01	0.71 ± 0.01
S3	0.59 ± 0.01	—
S4	0.68 ± 0.01	—
S5	0.64 ± 0.01	—
S6 (pre)	0.63 ± 0.01	0.57 ± 0.01
S6 (post)	0.64 ± 0.01	0.56 ± 0.02

uncertainty. The results of the WLS regression for all the series combined are shown in figures 9(*a*) and (*c*) and in table 4 for each scenario, together with the corresponding coefficient of determination R^2. The scaling factors for the NC and CFPD estimated by WLS regression by combining the data from all the series are $k_{NC} = 0.643 \pm 0.002$ with $R^2 = 0.952$ and $k_{PD} = 0.665 \pm 0.002$ with $R^2 = 0.812$ respectively. As for the individual series, the results in tables 3 and 4 are comparable within a few percent. A negative coefficient of determination for the CFPD in scenarios S1 and S6 is to be expected in cases where the linear regression is without a constant term, as done here (zero CRs are expected for zero predicted ones) and when the data weakly scale with each other. It is worth pointing out that a small or negative R^2 indicates simply that the regression in such cases is no better than a fit with a constant term independent of x. This can indeed be seen in figure 5(*b*) where ν_{PD} scales very weakly with ν_p in the case of scenario S_6 after the sawtooth crash. Nevertheless, even in such cases, the estimated regression parameter is an appropriate description of the deviation from the predicted CRs.

A closer inspection of figures 9(*b*) and (*d*) reveals that the NC measurements are affected by a small amount of heteroskedasticity while the CFPD is less affected. Although heteroskedasticity does not affect the estimate of the scaling factor from the WLS regression (which still remains an unbiased estimator), the estimate of the variance in k (and therefore the uncertainties δk) is biased and might not be accurately estimated. To address this issue, WLS regression has been applied to the log-transformed measured and predicted CRs of all series combined. In such a case, the scaling factors obtained are $k_{NC} = 0.46 \pm 0.03$ with $R^2 = 0.960$ and $k_{PD} = 0.61 \pm 0.05$ with $R^2 = 0.692$ respectively, indicating that uncertainty δk is a factor 10 larger than those predicted by WLS. The reason for obtaining a smaller k_{NC} is that log-transformed data have larger uncertainties for low CRs: in fact, an ordinary LS regression gives $k_{NC} = 0.59 \pm 0.08$ with $R^2 = 0.960$.

In conclusion, therefore, the scaling factor for both the NC and the CFPD is approximately $k = 0.6 \pm 0.1$.

5. Discussion

The observed CRs for the NC and the CFPD are difficult to reconcile with the measurement of the total neutron yield from the FC, even in the simplest quiescent scenarios. Since the same TRANSP/NUBEAM simulation is used to estimate ν_n,

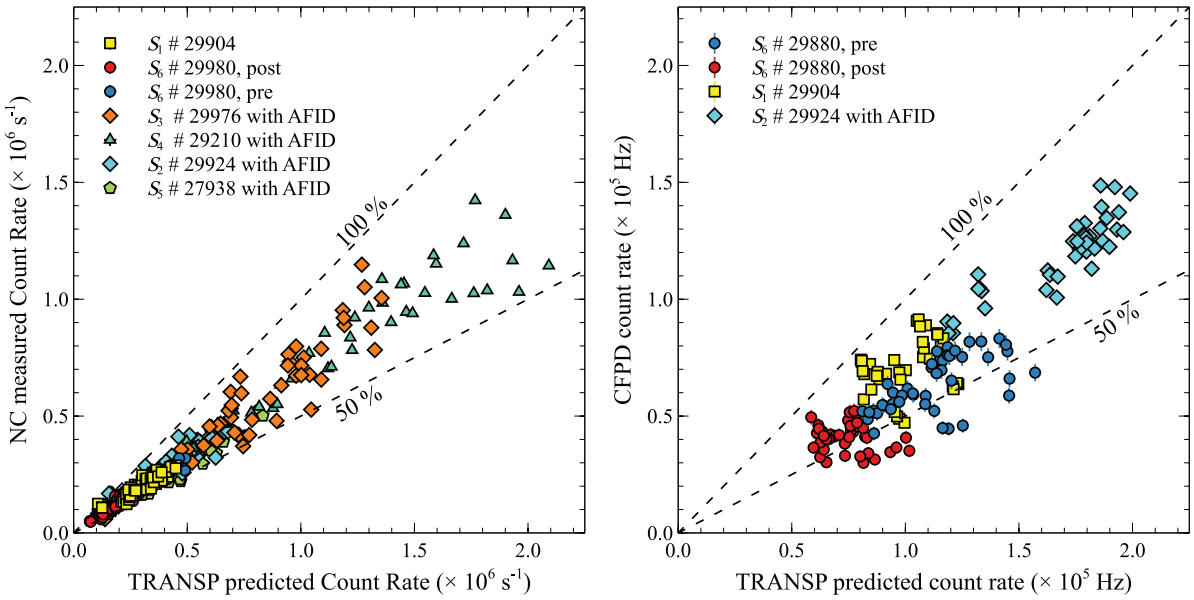

Figure 8. Comparison between TRANSP predicted and measured CRs by the neutron camera (left panel) and the charged fusion product detector (right panel). For scenarios S_2–S_5 characterised by strong TAE, FB and LLM activity, TRANSP predictions have been carried out by adjusting the anomalous fast ion diffusion coefficient D_a to match the FC measurements. Each data point represents the ratio between individual NC channels and the TRANSP predicted CRs for selected times during the plasma discharge. The labels 'pre' and 'post' refer to the time intervals before and after a sawtooth crash.

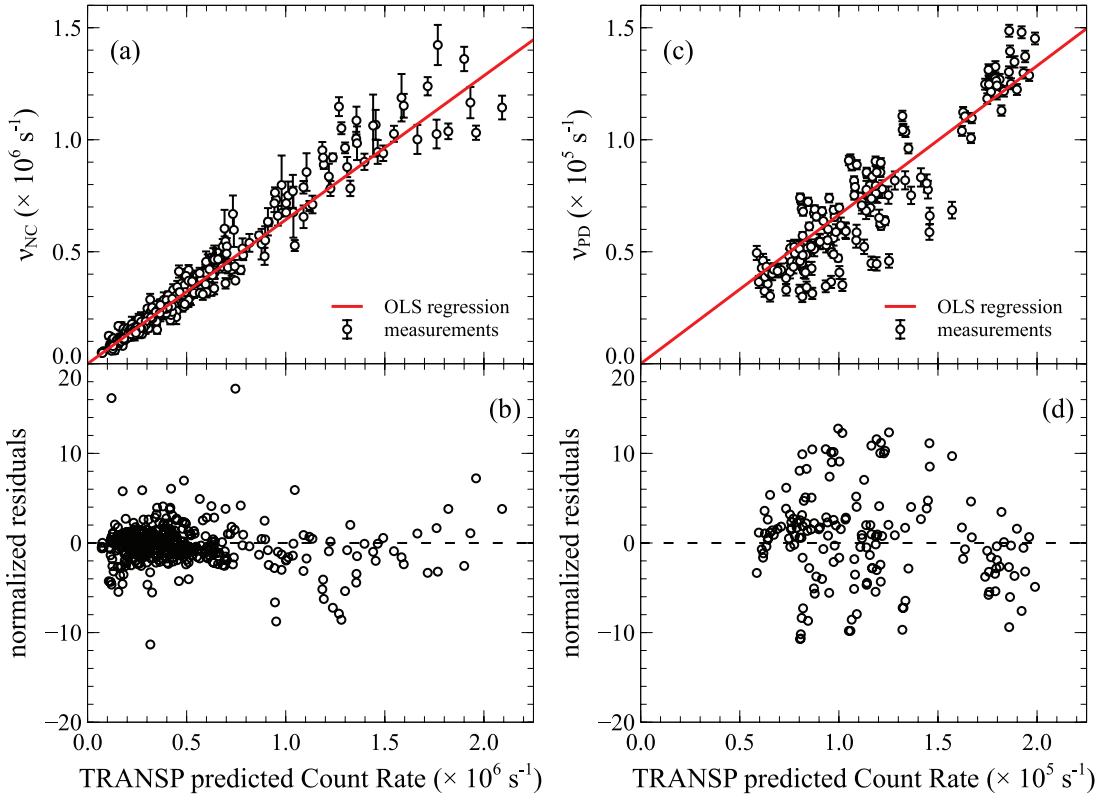

Figure 9. WLS regression between TRANSP predicted and measured CRs for the neutron camera (*a*) and the charged fusion product detector (*c*) for all series combined. The corresponding normalized residuals are shown in (*b*) and (*d*) respectively.

ν_p and Y_n, it is difficult to understand how the situation in which $Y_n = 0.9Y_{FC}$ and simultaneously $\nu_{NC}/\nu_n \approx \nu_{PD}/\nu_p \approx 0.6$ can arise. One possibility is that both the NC and CFPD efficiencies are wrongly estimated in such a way that results in a similar ratio between the predictions and measurements. Considering that the NC and CFPD are two totally independent diagnostics, relying on completely different physical principles, this seems implausible although it cannot be ruled out. An alternative explanation could be that the neutron emissivity used as the starting point for estimating the expected

Table 4. Estimate of the scaling factor for each scenario from neutron camera data (k_{NC}) and the CFPD (k_{PD}) using WLS regression. The labels 'pre' and 'post' refer to the time intervals before and after a sawtooth crash. The horizontal dash '—' indicates that CFPD measurements are not available.

Scenario	k_{NC}	R^2	k_{PD}	R^2
S1	0.670 ± 0.004	0.824	0.682 ± 0.003	−0.270
S2	0.672 ± 0.005	0.885	0.701 ± 0.002	0.780
S3	0.653 ± 0.004	0.856	—	—
S4	0.663 ± 0.004	0.941	—	—
S5	0.587 ± 0.005	0.882	—	—
S6 (pre)	0.632 ± 0.007	0.954	0.550 ± 0.005	0.279
S6 (post)	0.571 ± 0.007	0.709	0.527 ± 0.006	−1.227

CRs for both the NC and CFPD is incorrect. However, as discussed in section 3.2, the neutron emissivity calculated by TRANSP/NUBEAM agrees very well with the one calculated by DRESS, starting from the same underlying fast ion distribution function. In addition, if the neutron emissivity was to be wrong, then it would be impossible for the FC to match the TRANSP/NUBEAM predictions for the total neutron yield.

An entirely different explanation for the disagreement between FC and the fusion product measurements is to assume that the original calibration of the FC and its subsequent tracking via activation foils has become unreliable. A close scrutiny of the absolute calibration described in [18] identified a few issues that might contribute to this. The first is the lack of the absolute calibration of the ^{252}Cf source which, as stated by the authors of the calibration study, has been calibrated only once 20 years before using a method known to be accurate to about 2%. The calibration of the FC on MAST was then performed, correcting for the decay of the source using the published half-life of the isotope and assuming the same 2% uncertainty in the result as obtained for the original calibration. It is noted that a single point calibration of a ^{252}Cf source is not sufficient to determine its isotopic composition and, therefore, the proportion of the isotope ^{250}Cf was not known at the time of the original source calibration. An isotopic composition different to that assumed might alter the strength of the neutron source, especially as it ages [33], thus representing an additional, unquantified uncertainty in source strength. A second source of uncertainty in the FC calibration concerns the relative simplicity of the MCNP model used to translate the ^{252}Cf neutron emission to the counts on the FC. The accuracy of the MCNP calculation depends on the detail of the model and the time available for running the code. The model used omitted some details, such as the wooden floor around the top of the machine and vessel ports and coil supports, leading to an estimate of the error in the MCNP calculation of 8% arising from the combination of the model setup and the Monte-Carlo statistics. When comparing the MCNP results to the ^{252}Cf measurements, the counts predicted were larger than those observed in the FC by a factor of between 24 and 33 with the difference in the scaling factors being dependent on the toroidal position of the ^{252}Cf source. The magnitude of the scaling factors was ascribed to a high acquisition threshold in the electronics attached to the FC and could therefore be normalised using an average factor of 27. However, the position-dependent variation in the scaling factors (in the range ±17%) does not appear to be fully explained by the aforementioned contributions to the total uncertainties in the measurements and modelling. It is also recognised that significant changes to MAST have occurred since this original calibration, most notably the installation of the divertor structure that has most likely altered the neutron field. Finally, the cross-calibration with the activation foil is only indicative as the neutron flux on and the activation of the indium foil were not simulated in MCNP. It is also recognised that one of the principal purposes of the FC measurement is to track the total neutron dose in the shielded machine area for safety purposes, particularly tracking the activation of machine components to ensure this is below the allowed limits. The total neutron dose was assessed after each experimental campaign and, in each case, it was found that the dose measured by the FC was higher than that averaged between 12 CR39 neutron monitor badges in the shielded area. It was concluded that, although the FC measurement did not agree with the badge measurements, operations could safely continue without requiring a re-calibration of the FC. The absolute calibration of an FC on a tokamak is a very complicated endeavour, as the recent calibration in JET has highlighted [2]. The points above suggest additional sources of uncertainty in the MAST FC absolute calibration.

Unfortunately, even leaving aside the comparison with the FC measurements, the experimental observations presented in this work indicate that one or multiple systematic error(s) are present in either the NC and CFPD diagnostics or in the TRANSP/NUBEAM inputs and modelling. In section 4.1, it was shown that it is possible to remove the discrepancy by changing, one at a time, the plasma parameters that affect the neutron emissivity, such as the effective charge, the electron temperature, the NBI energy and density. However, the required changes are much larger than the accepted uncertainties in these quantities which are therefore discounted as the source of the observed discrepancy. Even envisaging a situation in which Z_{eff}, T_e, E_{NBI} and n_{NBI} are changed simultaneously within their experimental uncertainty and in the right direction so that predicted and measured CRs agree would not be sufficient to resolve the observed discrepancy. In particular, the NBI energy has been confirmed by measurements of the Doppler shift of the fast ion D-α (FIDA) emission. In fact, a detailed review of the NBI power and species fraction calibration was carried out in the same period as the plasma discharges studied here. The NBI calibration included in-vessel spectroscopic measurements using specific beam-into-gas

plasma discharges to determine the NBI species fractions and injection energy. The NBI power was measured internally in the beamlines using the water-flow calorimetry method using data from the *in situ* beamline calorimeters. Losses due to beam scraping and to re-ionisation in the beamline were estimated using simulation codes which have proved highly reliable in extensive testing and use over many years on the JET NBI test-bed. Since fusion reactions are primarily produced in beam–target interactions by the NBI full-energy component, the full-energy component would need to be reduced by an amount similar in magnitude to the observed neutron discrepancy to match TRANSP/NUBEAM predictions with the experimental observations, which is not credible. In addition, given the accuracy of the spectroscopic measurements carried out in determining the species fractions, any contribution to the observed discrepancy from these uncertainties in the NBI mixing fractions is considered to be small. Regarding the absolute intensity of the FIDA signal, related to the NBI intensity, some uncertainties remain which will require further investigation: these will be addressed in a future work. In particular, the role of the halo neutrals during NBI heating has a significant impact on the intensity of both FIDA and NPA signals [34] and was not included in the original FIDA/FIDAsim benchmarking [29]. The stored plasma kinetic energy W is an additional plasma parameter that is typically used to check the quality of TRANSP/NUBEAM simulations. On MAST, W is strongly dependent on the NBI heating which contributes to approximately 35% of its total value [35] and therefore can provide an additional check on the calculated neutron emissivity. Unfortunately on MAST, the diamagnetic loop that is typically used to measured the stored energy was not available for the plasma discharges used in this study.

Losses of fast ions due to charge-exchange processes have been investigated in TRANSP/NUBEAM by modifying both the edge neutral deuterium flux and the external neutral deuterium density $n_{0,\mathrm{ext}}$. In both cases, these quantities have been increased by one order of magnitude with respect to their reference values and no significant difference in the neutron yield was observed. For example, on MAST, a fast pressure gauge provides an indication of the neutral molecular deuterium density which, for the plasma scenarios studied here, varied in the range 1×10^{18}–1×10^{19} m^{-3} depending on the level of gas puff, but no change in the neutron yield was observed when setting $n_{0,\mathrm{ext}} = 1 \times 10^{20}$ m^{-3}. It is possible that even higher values of $n_{0,\mathrm{ext}}$ might result in a reduction in Y_n, but such a high density for the neutral D gas is unlikely, especially near the last closed flux surface where most of the charge exchange processes between confined fast ions and neutral atoms and molecules would occur. For example, in NSTX, the atomic and molecular deuterium density have been estimated to be less than 1×10^{17} and 1×10^{18} m^{-3} with both approaching the atomic density level close to the plasma boundary [36]. On START, a very high neutral density was estimated (approximately 1×10^{19} m^{-3}) and was considered as a consequence of the very small ratio between the plasma and the vessel volume (about 7%) [37]; for comparison, the same ratio for NSTX is approximately 50% and about 20% on MAST.

The role of toroidal field ripples (TFRs) on the loss of fast ions in MAST is briefly reviewed here. In an initial study, in which a full orbit particle tracking code was used, it was found that TFRs have a negligible impact on fast ion confinement [38]. However, in a more recent study specifically devoted to the neutron emission modelling along a fast ion trajectory using a non-steady state full orbit following code, it was suggested that TFRs have a significant role in reducing the confinement of fast ions [6, 7]. In particular, this study suggests a possible explanation for the discrepancy between measured and TRANSP/NUBEAM predicted neutron CRs. In NUBEAM fast ions, orbits are calculated using the guiding-centre approximation combined with a finite Larmor radius correction algorithm to account for the significant size of the Larmor radii of fast ions in MAST compared with the plasma volume and the scale of the spatial gradients of the plasma profiles. Even with this finite Larmor radius correction in place, however, the DD fusion reactivity is larger than that calculated when a full orbit following code is used instead [6, 7]. The reason for this is that the size of the fast ion orbits is not negligible compared to the variation in the thermal deuterium density profile. According to this work, the reduction in the neutron yield between the guiding-centre (NUBEAM) and full orbit estimates is approximately 30%, giving a ratio of approximately 0.7 not far from the discrepancy here reported. These findings are also supported by an initial comparison between the fast ion density profile and NBI power deposition in MAST calculated with TRANSP/NUBEAM and ASCOT [39]. ASCOT [40] can evaluate the fast ion trajectories in both guiding-centre and full-orbit modes. In this study, it was found that in plasma discharges with little MHD activity, for which D_a was used (#26 887), the fast ion density and NBI power deposition profiles were quite similar when ASCOT was operated in guiding-centre mode. However, when ASCOT was run in full-orbit mode, the fast ion density profile was approximately 50% of the one predicted by TRANSP/NUBEAM. Note that, in this comparison, the same plasma profiles were used in both TRANSP/NUBEAM, while the magnetic equilibria were calculated internally by both codes and were slightly different.

An additional possible source of fast ion redistribution (in addition to classical collisions), which could be present even in a quiescent scenario, and that is not directly modelled in TRANSP, might be fast ion transport driven by micro-turbulence. However, this should not play a major role in STs since the fast ion large Larmor radius would cancel out the effect of micro-turbulence. Even in a case where turbulence causes transport, as observed in the DIII-D tokamak [41], it should affect the low energy fast ions in the $E_\mathrm{NBI}/T_\mathrm{i,e} \ll 10$ range and at a large minor radius, while our observations indicate that, in particular, the most energetic fast ions (for which $E_\mathrm{NBI}/T_\mathrm{i,e} \gg 10$) are redistributed across the entire radial profile. Even in such cases, the fast ion transport driven by turbulence is much smaller than the Alfvénic transport [42]. As far as the authors are aware, no observation of micro-turbulence driven fast ion redistribution has been reported in STs. As a result, it seems implausible that micro-turbulence might be

responsible for the observed large discrepancy reported in MHD quiescent scenarios.

6. Conclusions

Neutrons and protons in MAST NBI heated plasmas are produced mainly by beam-thermal reactions (≈90%) and, to a lesser extent, by beam–beam reactions (≈10%) with a negligible contribution from thermal fuel reactions. The fusion product deficit reported in this work is independent of the MAST plasma scenario and approximately of the order of 40%. This discrepancy cannot be explained by the uncertainties in the input data to TRANSP/NUBEAM codes unless a large systematic error in one or more such parameters has so far gone undetected. This seems rather unlikely as MAST diagnostics and NBI systems have been well calibrated and validated. The only exception is the FC, whose absolute calibration might have changed over time, leading to a coincidental agreement with TRANSP/NUBEAM predictions of the total neutron rate. It might still be the case that systematic errors are present both in the NC and CFPD, but the fact that two independent diagnostics observe a similar deficit in the fusion products from two different channels of the DD reaction makes this quite unlikely. The fact that both the NC and CFPD synthetic diagnostics use the same neutron emissivity profile to estimate the predicted CRs hints at the possibility of its systematic overestimation by TRANSP/NUBEAM. However, the neutron emissivity profile calculated by TRANSP/NUBEAM and by DRESS agree within 1%, suggesting that the actual quantity that is overestimated is the fast ion density. On the other hand, FIDA diagnostic measurements of the total fast ion density in MAST agree with TRANSP/NUBEAM estimates [29]. However, uncertainties in the absolute calibration of the FIDA diagnostic cannot rule out that this agreement is fortuitous, especially considering the lack of proper modelling in TRANSP/NUBEAM of the role of the halo neutrals. Assuming that the NC and CFPD measurements are correct, one possible source of the discrepancy that we have identified in this work is the guiding centre approximation used in NUBEAM that was shown to lead to an overestimation of the fast ion density profile [39] and the local neutron emissivity compared to the one calculated by a full orbit following code [6]. This effect is very important in spherical tokamaks due to the large Larmor radius of fast ion orbits compared with the plasma dimensions and the thermal fuel density profile gradients. Instead, on conventional tokamaks with much stronger magnetic fields, the guiding centre approximation might be sufficiently good for neutron rate predictions and measurements to agree, although a careful choice of the effective charge is required [43]. This might explain why, on MAST, the fusion product deficit is scenario independent, contrary to that observed on JET where other factors might be at play. Further work is needed to better understand and explain the discrepancy between not only fusion product predictions and measurements but also between the NC and CFPD observations with those of the FC and FIDA diagnostics. In this respect, a collaboration has been established with the Princeton Plasma Physics Laboratory to undertake more extensive validation and verification of the TRANSP/NUBEAM codes, in particular, regarding the impact on the fusion reaction rates of the equilibrium solver (which at times can produce unphysical q-profiles), of the spatial mapping of the experimental profiles (usually given as a function of normalized radius rather than actual major radius) and on the role of halo neutrals [34] on the fusion reaction rates. In addition, the modelling of the fusion product diagnostics using full orbit following codes, such as ASCOT and LOCUST-GPU [44], would help to settle the issue: this will be the subject of a follow-up investigation.

Acknowledgments

This work was funded by the Swedish Research Council, the RCUK Energy Programme under grant EP/I501045, the European Union's Horizon 2020 Research and Innovation Programme under grant agreement number 633053 and the US Department of Energy Contract number DE-SC0001157. The views and opinions expressed herein do not necessarily reflect those of the European Commission. The authors are grateful to O. Jones (CCFE) and C. Michael (Australian National Univeristy, Canberra) for discussion on the MAST FIDA diagnostic, to M. Fitzgerald and R. Akers (CCFE) for their help with TRANSP/NUBEAM modelling, to K.G. McClements (CCFE) for fruitful discussions on the role of toroidal field ripples and guiding-centre approximations, and J. Harrison and S. Henderson (CCFE) for their support in the analysis of spectroscopic measurements. The authors are also grateful to M. Gorelenkova, F. Poli and M. Podestà of PPPL for their support and help with the TRANSP/NUBEAM simulations.

ORCID iDs

M. Cecconello https://orcid.org/0000-0002-2571-1920

References

[1] Weisen H. *et al* 2017 *Nucl. Fusion* **57** 076029
[2] Syme D. *et al* 2014 *Fusion Eng. Des.* **89** 2766–75
[3] Goldston R.J. *et al* 1981 *J. Comput. Phys.* **43** 61
[4] Pankin A., McCune D., Andre R., Bateman G. and Kritz A. 2004 *Commun. Comput. Phys.* **159** 157
[5] Herschbach K., Maurer W., Maurer W. and Vetter J.E. (Eds.) 1995 *Fusion technology 1994 Proceedings* vol 1 (Amsterdam: Elsevier)
[6] Tani K. *et al* 2016 *Plasma Phys. Control. Fusion* **58** 105005
[7] McClements K., Tani K., Akers R.J., Liu Y.Q., Shinohara K., Tsutsui H. and Tsuji-Iio S. 2018 *Plasma Phys. Control. Fusion* **60** 095005
[8] Cecconello M. *et al* 2015 *Plasma Phys. Control. Fusion* **57** 014006
[9] Cecconello M. *et al* 2014 *Nucl. Instrum. Methods Phys. Res.* A **753** 72–83
[10] Perez R.V. *et al* 2014 *Rev. Sci. Instrum.* **85** 11D701
[11] Goorley T. *et al* 2012 *Nucl. Technol.* **180** 298–315

[12] Klein H. and Neumann S. 2002 *Nucl. Instrum. Methods Phys. Res.* A **476** 132–42
[13] Bähr C., Böttger R., Klein H., von Neumann-Cosel P., Richter A., Schmidt D., Schweda K. and Strauch S. 1998 *Nucl. Instrum. Methods Phys. Res.* A **411** 430–6
[14] Schweda K. and Schmidt D. 2002 *Nucl. Instrum. Methods Phys. Res.* A **476** 155–9
[15] Weber C., Fabry I., Huhn V., Siepe A. and von Witsch W. 2002 *Nucl. Instrum. Methods Phys. Res.* A **488** 307–13
[16] Dietze G. and Klein H. 1982 *Technical Report* Physikalisch-Technische Bundesanstalt Braunschweig, PTB-ND-22, Germnany
[17] Lao L., Ferron J., Groebner R., Howl W., John H.S., Strait E. and Taylor T. 1990 *Nucl. Fusion* **30** 1035
[18] Stammers K. and Loughlin M. 2006 *Nucl. Instrum. Methods Phys. Res.* A **562** 521–30
[19] Klimek I. *et al* 2015 *Nucl. Fusion* **55** 023003
[20] Eriksson J., Conroy S., Sundén E.A. and Hellesen C. 2016 *Comput. Phys. Commun.* **199** 40–6
[21] Bosch H.S. and Hale G. 1992 *Nucl. Fusion* **32** 611
[22] Heidbrink W.W. and Strachan J.D. 1985 *Rev. Sci. Instrum.* **56** 501–18
[23] Qu Z.S., Fitzgerald M. and Hole M.J. 2014 *Plasma Phys. Control. Fusion* **56** 075007
[24] Gorelenkov N. and Zakharov L. 2018 *Nucl. Fusion* **58** 082031
[25] Jones O.M. *et al* 2015 *Plasma Phys. Control. Fusion* **57** 125009
[26] Cecconello M., Sperduti A. and The MAST team 2018 *Plasma Phys. Control. Fusion* **60** 055008
[27] Scannell R. *et al* 2008 *Rev. Sci. Instrum.* **79** 10E730
[28] Patel A., Carolan P.G., Conway N.J. and Akers R.J. 2004 *Rev. Sci. Instrum.* **75** 4944–50
[29] Michael C.A. *et al* 2013 *Plasma Phys. Control. Fusion* **55** 095007
[30] Heidbrink W., Ruskov E., Liu D., Stagner L., Fredrickson E., Podestà M. and Bortolon A. 2016 *Nucl. Fusion* **56** 056005
[31] Podestà M., Gorelenkova M., Darrow D., Fredrickson E., Gerhardt S. and White R. 2015 *Nucl. Fusion* **55** 053018
[32] Zeeland M.A.V. *et al* 2011 *Phys. Plasmas* **18** 056114
[33] Roquemore A.L. Darrow S.D. and Medley S.S. 2011 Absolute calibration of the NSTX neutron monitor system *lEEE/ NPSS 24th Symposium on Fusion Engineering (Chicago, USA, 26–30 June 2011)* SPI -39 (https://doi.org/10.1109/SOFE.2011.6052263)
[34] Medley S.S., Liu D., Gorelenkova M.V., Heidbrink W.W. and Stagner L. 2016 *Plasma Phys. Control. Fusion* **58** 025007
[35] Akers R.J. *et al* 2003 *Plasma Phys. Control. Fusion* **45** A175
[36] Stotler D.P., Scotti F., Bell R.E., Diallo A., LeBlanc B.P., Podestà M., Roquemore A.L. and Ross P.W. 2015 *Phys. Plasmas* **22** 082506
[37] Akers R. *et al* 2002 *Nucl. Fusion* **42** 122
[38] McClements K.G. and Hole M.J. 2012 *Phys. Plasmas* **19** 072514
[39] Asunta O., Akers R., Corrigan G., Keeling D., Kurki-Suonio T., Muir D., Romanelli M., Salmi A. and Turnyanskiy M. 2012 *39th EPS Conf. and 16th Int. Congress on Plasma Physics (Stockholm, Sweden, 2–6 July 2012)* p P1.006 (http://ocs.ciemat.es/EPSICPP2012PAP/pdf/P1.006.pdf)
[40] Kurki-Suonio T. *et al* 2009 *Nucl. Fusion* **49** 095001
[41] Heidbrink W.W., Park J.M., Murakami M., Petty C.C., Holcomb C. and Van Zeeland M.A. 2009 *Phys. Rev. Lett.* **103** 175001
[42] Duarte V.N., Berk H.L., Gorelenkov N.N., Heidbrink W.W., Kramer G.J., Nazikian R., Pace D.C., Podestà M. and Van Zeeland M.A. 2017 *Phys. Plasmas* **24** 122508
[43] Tardini G., Höhbauer C., Fischer R., Neu R. and the ASDEX Upgrade Team 2013 *Nucl. Fusion* **53** 063027
[44] Akers R.J., Verwichte E., Martin T.J., Pinches S.D. and Lake R. 2012 *9th EPS Conf. on Plasma Physics 16th Int. Congress on Plasma Physics (Stockholm, 2–6 July 2012)* p P5.088 (http://ocs.ciemat.es/epsicpp2012pap/pdf/P5.088.pdf)